


Label-Free Electrochemical Monitoring of Concentration Enrichment during Bipolar Electrode Focusing

Eoin Sheridan,[†] Dzmitry Hlushkou,[‡] Robbyn K. Anand,^{†,⊥} Derek R. Laws,[†] Ulrich Tallarek,^{*,‡} and Richard M. Crooks^{*,†}

[†]Department of Chemistry and Biochemistry, Center for Electrochemistry, and the Center for Nano- and Molecular Science and Technology, The University of Texas at Austin, 1 University Station, A5300, Austin, Texas 78712-0165, United States

[‡]Department of Chemistry, Philipps-Universität Marburg, Hans-Meerwein-Strasse, 35032 Marburg, Germany

 Supporting Information

ABSTRACT: We show that a label-free electrochemical method can be used to monitor the position of an enriched analyte band during bipolar electrode focusing in a microfluidic device. The method relies on formation of a depleted buffer cation region, which is responsible for concentration enrichment of the charged analyte. However, this depletion region also leads to an increase in the local electric field in the solution near a bipolar electrode (BPE), and this in turn results in enhanced faradaic reactions (oxidation and reduction of water) at the BPE. Therefore, it is possible to detect the presence of the concentrated analyte band by measuring the current passing through the BPE used for concentration enrichment, or the concentrated band can be detected at a secondary BPE dedicated to that purpose. Both experiments and simulations are presented that fully elucidate the underlying phenomenon responsible for these observations.



In previous reports we demonstrated that charged analytes can be concentrated up to 500 000-fold using a method we call bipolar electrode focusing (BEF).^{1–6} In these earlier studies the concentrated analyte was detected using fluorescence, but here we show that electrochemical methods are also capable of detecting enriched bands of charged species. Additionally, we provide theoretical and experimental insights into the nature of the observed electrochemical signal. The significant achievement is that both enrichment and detection are now electrochemical, thereby eliminating the need for fluorescent labeling and detection. Importantly, the analyte being detected does not itself need to be electroactive.

The basis of BEF is manipulation of the local electric field within an electrolyte solution in the vicinity of a bipolar electrode (BPE).^{3–6} In brief, application of a voltage (E_{tot}) across a buffer-filled microchannel of length l_{channel} , results in an electric field having a constant value of $\sim E_{\text{tot}}/l_{\text{channel}}$. If a BPE is present in the channel (Scheme 1a), and if E_{tot} is sufficiently large, faradaic electrochemical reactions will occur at the poles of the BPE (Scheme 1b). This situation is satisfied when the fraction of E_{tot} dropped over the length of the BPE ($\Delta E_{\text{elec}} = E_{\text{tot}}(l_{\text{elec}}/l_{\text{channel}})$, where l_{elec} is the length of the BPE) exceeds that required to drive a reduction reaction at the cathodic pole and an oxidation at the anodic pole.^{3–6} The key point is that the interfacial potential between the poles of the BPE and the solution is determined by E_{tot} . The potential of the BPE is also a function of E_{tot} and therefore will adjust to the surrounding solution potential.

Electrochemical processes may result in substantial changes to the ionic strength of the buffer near the BPE. For example, in the

experiments reported here, the buffer is Tris. Water oxidation at the BPE cathode generates OH^- , which neutralizes TrisH^+ , thereby depleting charge carriers in solution and creating an electric field gradient near the BPE. Additional information about the faradaic reactions occurring at the BPE are provided in the Supporting Information. Enrichment of analyte anions occurs at the position on the electric field gradient where the velocity due to total flow (nearly uniform along the length of the channel) is exactly balanced by an equal and opposite electrophoretic velocity (which is a function of location along the electric field gradient), where total flow is due to electroosmosis (EOF) and pressure-driven flow (PDF) combined. This process is illustrated in Scheme 1c.

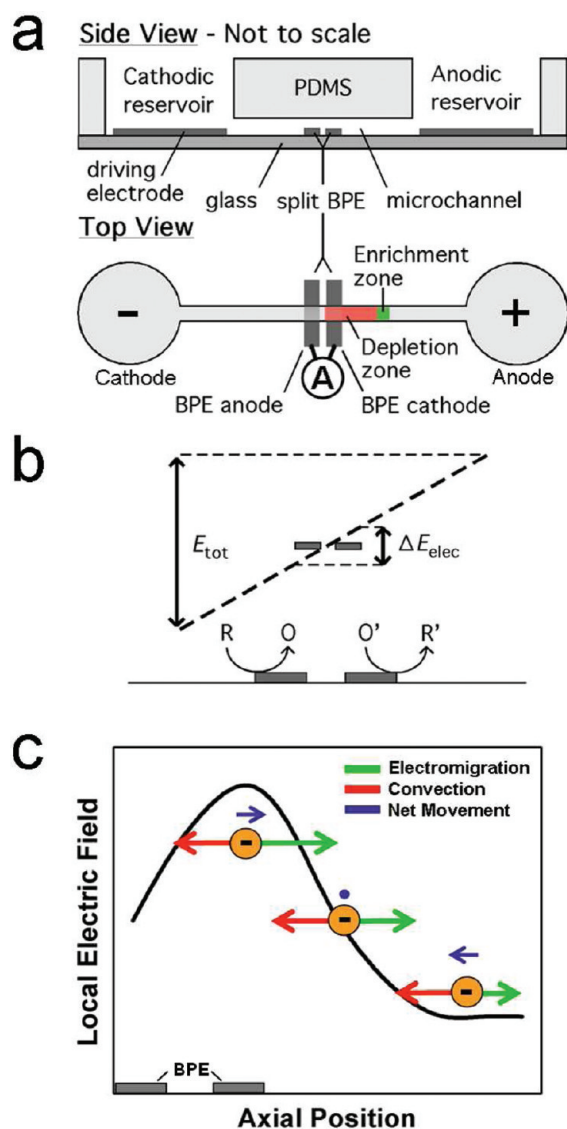
Microfluidic-based sensors having multiple, integrated functions are now commonplace.^{7–10} However, in some cases the limit of detection of these systems is compromised by small analysis volumes and low analyte concentrations. One approach for addressing this problem involves enrichment of the analyte at a specified location, for example, near the detector. Many approaches for sample enrichment have been reported, including electrokinetic membrane filtration,^{11,12} solid-phase extraction (SPE),^{13,14} isoelectric focusing (IEF),^{15–17} and temperature gradient focusing (TGF).^{18,19} BEF is a form of electric field gradient focusing (EFGF), an approach for microfluidic concentration enrichment that is frequently used in chip-based analytical devices.^{20–27} Enrichment factors of up to 10^7 have been reported using other members of the EFGF family.²⁷

Received: June 2, 2011

Accepted: July 20, 2011

Published: August 04, 2011

Scheme 1



Here we present a method for monitoring the location of an analyte band enriched using BEF by measuring the current passing through the BPE (i_{BPE}). Specifically, enrichment is initiated by connecting the two poles of a split BPE through an ammeter and then applying a sufficiently high E_{tot} to initiate enrichment of an anionic fluorescent tracer (Scheme 1). This configuration makes it possible to simultaneously monitor the location of the enriched band using both fluorescence microscopy and i_{BPE} . Also, additional microband electrodes present within the channel make it possible to quantitatively measure the electric field gradient in the vicinity of the BPE.³ This provides insight into the underlying principles of electrochemical detection. Numerical simulations are in accord with the experimental results.

EXPERIMENTAL SECTION

Chemicals. Poly(dimethylsiloxane) (PDMS) channels were prepared using a Sylgard 184 elastomer kit obtained from K. R. Anderson, Inc. (Morgan Hill, CA). Au-coated glass slides (100 nm thick, no adhesion layer) were purchased from EMF

Corp. (Ithaca, NY). The fluorescent tracer was 4,4-difluoro-1,3,5,7,8-pentamethyl-4-bora-3a,4a-diaza-*s*-indacene-2,6-disulfonic acid, disodium salt (BODIPY²⁻, Invitrogen Corp., Carlsbad, CA). Pluronic F-108 was obtained from BASF (Florham Park, NJ). Tris buffer (pH 8.1) was prepared by dilution of a 1.0 M Tris-HCl solution purchased from Fisher (Fair Lawn, NJ). Photoresist (AZ 4620) and developer (AZ 421 K) were purchased from AZ Electronic Materials (Somerville, NJ). All chemicals were used as received. Deionized water having a resistivity greater than 18 M Ω ·cm was used for all experiments (Milli-Q gradient system, Millipore, Bedford, MA).

Microfluidic Device Fabrication. Device fabrication has been described previously.^{3,4} Briefly, the driving electrodes and BPEs were deposited onto the glass base of the microfluidic device using standard photolithographic techniques. The driving electrodes consisted of microfabricated Au disks located at the bottoms of the two reservoirs. They were connected to a power supply via external contacts. An array of 15 gold microband electrodes consisting of 30 μ m wide lines and 50 μ m wide spaces was used to form the BPEs and measure the electric field gradient. The microbands had external contacts so that any two could be connected to form a BPE.

Microchannels were fabricated in PDMS using a previously described replica molding procedure.^{3,28} Briefly, a microfluidic channel (6 mm long, 100 μ m wide, and 21 μ m high) spanning two 5.0 mm diameter reservoirs was fabricated from PDMS. The PDMS was rinsed with ethanol and dried under N₂, and next both the PDMS and the glass slide supporting the Au electrodes were exposed to an O₂ plasma (60 W, model PDC-32G, Harrick Scientific, Ossining, NY) for 30 s on the medium power setting. After joining the PDMS replica and the glass slide, the entire assembly was placed in an oven at 70 °C for 7 min to promote irreversible bonding.

Modification of the channel walls with Pluronic was carried out using a previously reported method.²⁹ Specifically, the microfluidic devices were loaded with a 3.0 μ M, buffered Pluronic solution and allowed to equilibrate for 20 h at 23 \pm 2 °C. The channels were then thoroughly rinsed with pure buffer solution and used immediately without further treatment. Modification of the channel walls with Pluronic lowered EOF mobility (μ_{EOF}) from 4.5 \times 10⁻⁸ to 3.6 \times 10⁻⁹ m²/(V s), such that when 25 V was applied the EOF velocity (v_{EOF}) was 15 μ m/s.

Instrumentation and Data Acquisition. Fluorescence images were obtained using a Nikon AZ100 (Nikon Co., Tokyo, Japan) microscope equipped with a mercury lamp (Nikon) and a CCD camera (Cascade, Photometrics Ltd., Tucson, AZ). Micrographs were processed using V++ Precision Digital Imaging software (Digital Optics, Auckland, New Zealand). Images were captured using 1 \times 1 binning with 512 \times 290 pixels and a 100 ms exposure time. Fluorescence intensities for calibration curves were obtained using a function that averages intensities of all pixels along one axis of the region of interest. Fluorescence intensities of concentrated analytes were obtained using a maximum function, which provides the maximum intensity values along one axis of the region of interest.

Concentration Enrichment Experiments. Prior to each enrichment experiment, the microfluidic channel was rinsed by introducing 80.0 μ L of 5.0 mM Tris buffer (pH 8.1) into the anodic reservoir and 15.0 μ L into the cathodic reservoir. The buffer solution was allowed to flow through the microchannel for 20 min in response to the solution height differential. Next, the rinsing solution in each of the reservoirs was replaced with 80.0 μ L of 1.0 μ M

BODIPY²⁻ in 5.0 mM Tris. Additional microliter increments of the same solution were added to each reservoir in individual experiments as indicated in the Results and Discussion section.

The concentration enrichment experiments themselves were carried out as follows. First, two microband electrodes having the desired separation (typically 500 μm) were connected via a conductive wire or ammeter. Second, a driving voltage ($E_{\text{tot}} = 25.0 \text{ V}$) was applied across the microchannel using a high-voltage power supply (LLS9120, TDK-Lambda Americas, Inc., San Diego, CA) connected to the microfabricated gold driving electrodes spanning the bottoms of the reservoirs. Measurements of i_{BPE} and fluorescence were obtained as a function of time. The PDF rate in the microchannel was estimated after each experiment by switching off E_{tot} and observing the movement of the enriched band under the influence of PDF only.

Current Measurements. The value of i_{BPE} was measured by connecting the pair of microbands defining the BPE via an ammeter (model 6517B electrometer, Keithley Instruments, Inc., Cleveland, OH). Data were processed using LabView software (National Instruments, Austin, TX). The total current flowing through the channel (i_{tot}) was measured in parallel with i_{BPE} by monitoring the voltage drop across a 523 k Ω resistor placed in series with the microchannel. The voltage was measured using a hand-held, digital multimeter equipped with PC-Link software (VA18B, Sinometer Instruments, ShenZhen, China).

Electric Field Profile Measurements. The axial electric field profile within the channel was monitored using a scanning digital multimeter (SDMM, model 2700, Keithley Instruments, Inc., Cleveland, OH) equipped with a multiplexer module (model 7701, Keithley) connected to all the microband electrodes except those defining the BPE. The SDMM was controlled with Microsoft Excel via the software provided by the SDMM manufacturer (ExceLinx, Keithley). The SDMM was interfaced to the microband electrodes through a breakout board (screw terminals). The SDMM reads the difference between pairs of microbands in sequence. The acquisition time for each voltage measurement was $\sim 0.1 \text{ s}$, and the voltage between pairs of microbands was read every 2.0 s. Electric field monitoring experiments proceeded as follows. First, the two halves of the BPE were connected via a conductive wire or ammeter. Second, the SDMM was placed into scan mode. Third, a driving voltage ($E_{\text{tot}} = 25.0 \text{ V}$) was applied across the microchannel via the driving electrodes. The captured data were stored and plotted as voltage differences between each microband pair versus time in real time using Excel.

Computer Simulations. Numerical simulations were used to model the local electric field and species concentration distributions in the microchannel.

The basic equations governing the physical phenomena in the system are the coupled Nernst–Planck (eq 1), Poisson (eq 2), and Navier–Stokes (eq 3) equations.

$$\frac{\partial c_i}{\partial t} = \nabla \cdot \left[D_i \nabla c_i + \frac{z_i F}{RT} \nabla \cdot (D_i \nabla \phi) - c_i v \right] + r_i \quad (1)$$

$$\nabla^2 \phi = - \frac{F}{\epsilon_0 \epsilon_r} \sum_i z_i c_i \quad (2)$$

$$\rho \left(\frac{\partial v}{\partial t} + v \cdot \nabla v \right) = - \nabla p + \mu \nabla^2 v - (\nabla \phi) \sum_i z_i c_i \quad (3)$$

Here, c_i is the concentration of species i (mol/m^3); D_i and z_i are its diffusion coefficient and valency, respectively; ϕ is the local

electric potential; F , R , and T represent the Faraday constant, molar gas constant, and absolute temperature, respectively; v is the flow velocity, r_i is the reaction term for species i ; ϵ_0 and ϵ_r are the vacuum permittivity and dielectric constant; ρ and μ are the mass density and dynamic viscosity of the liquid; p is hydrostatic pressure. The Nernst–Planck equation describes local mass and charge transport due to advection, diffusion, and electromigration; the Poisson equation establishes a relationship between the local electrical potential and the species concentration distribution; the Navier–Stokes equation relates the fluid flow velocity field to the pressure and Lorenz force.

The microchannel and reservoirs are assumed to be filled with 1.0 μM BODIPY²⁻ in 5.0 mM Tris–HCl buffer (pH 8.1). Thus, the species of interest include neutral Tris, its protonated form (TrisH⁺), Cl⁻, OH⁻, H₃O⁺, and BODIPY²⁻. The reaction terms in eq 1 take into account the fact that the local concentration of Tris, TrisH⁺, OH⁻, and H₃O⁺ can change due to the bulk buffer reactions and/or faradaic reactions.

The above formal description of the processes in the system was implemented as an iterative numerical scheme based on discrete spatiotemporal schemes optimized for parallel computations. In particular, for the solution of the Navier–Stokes, Poisson, and Nernst–Planck equations, the lattice-Boltzmann approach³⁰ and the numerical approaches described by Warren³¹ and by Capuani et al. were implemented.³² In all numerical schemes, a time step of 10^{-5} s and a space step of 10^{-6} m were used. The kinetics of the assumed faradaic and buffer reactions used in the simulations along with other details of the numerical implementation are provided in the Supporting Information. A single simulation required $\sim 14 \text{ h}$ using 64 processors of an SGI Altix 4700 supercomputer to analyze the temporal behavior of the system for 100 s.

RESULTS AND DISCUSSION

Relationship between BPE Current and Enriched Band Position. The device used for enrichment studies consisted of a 6 mm long microchannel containing an array of gold microbands (Figure 1a). Each microband was connected to an individual contact pad external to the device. BPEs of arbitrary length could then be formed by placing a jumper wire or ammeter across the external contact pads. In this example, a 500 μm long BPE was created by connecting two microbands through an ammeter so that i_{BPE} could be measured (Figure 1b) throughout the experiment.

The influence of the enriched band on i_{BPE} was investigated as follows. First, the microchannel was filled with 5.0 mM Tris buffer containing 1.0 μM BODIPY²⁻, and initially ($t = 0 \text{ s}$, Figure 1b) an excess (22.0 μL) of this solution was added to the anodic reservoir. Second, at $t = 50 \text{ s}$ a value of $E_{\text{tot}} = 25.0 \text{ V}$ was applied to the driving electrodes. At this point, the PDF rate resulting from the presence of unequal levels of solution in the two reservoirs results in a total flow rate toward the cathodic reservoir that is too fast to allow a stable depletion region to form in the vicinity of the BPE cathode. The Supporting Information provides more information about this situation, but the main point is that in the absence of a depletion region enrichment does not occur. This initial condition is important, because it makes it possible to observe the impact of initiating enrichment on i_{BPE} without changing E_{tot} . Figure 1b shows that immediately upon application of $E_{\text{tot}} = 25.0 \text{ V}$ an increase of i_{BPE} to $\sim 60 \text{ nA}$ is observed. This current arises from oxidation and reduction of

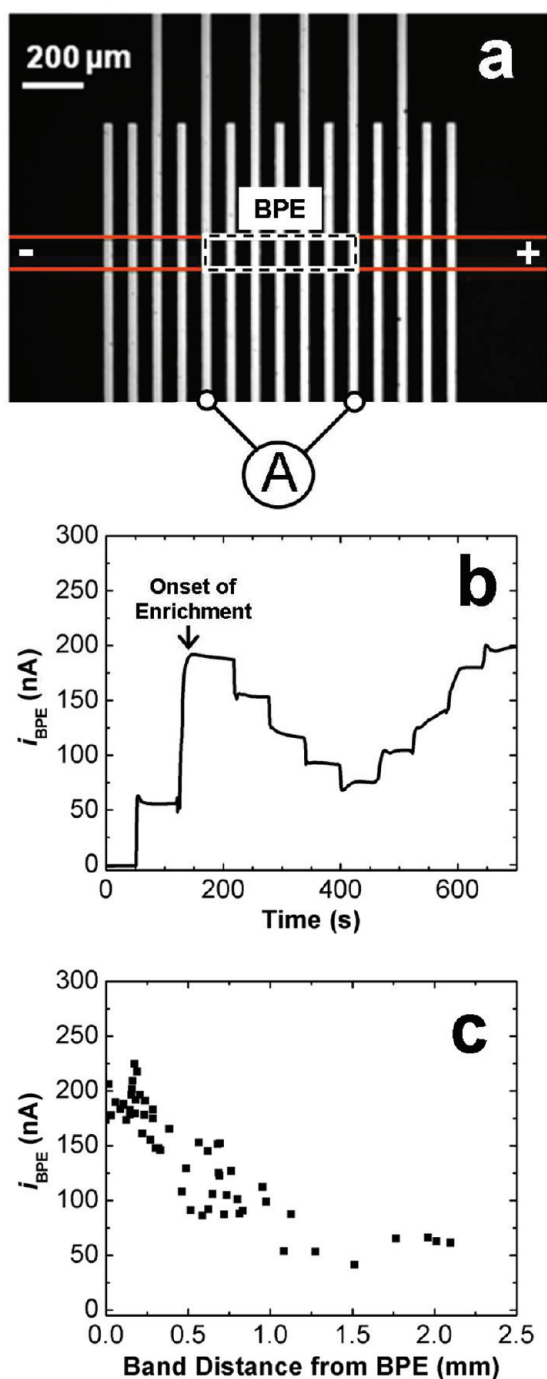


Figure 1. (a) Optical micrograph of gold microband electrodes that can be connected external to the channel to yield a BPE of arbitrary length. The current through the BPE (i_{BPE}) can be monitored by connecting the two poles of the BPE with an ammeter (A). (b) i_{BPE} as a function of time while an enriched BODIPY²⁻ band is formed and moved longitudinally in the channel by changing the total flow rate. (c) Relationship between i_{BPE} and the enriched BODIPY²⁻ band position. The initial concentrations in the microchannel were 5.0 mM Tris-HCl (pH 8.1) and 1.0 μM BODIPY²⁻. The BPE had a length of 500 μm .

water at the BPE anode and cathode, respectively (see the Supporting Information). Next, at $t = 120$ s, the original excess of solution in the anodic reservoir was partially offset by adding 4.0 μL to the cathodic reservoir. This results in a decrease in the

total flow rate from 245 to 205 $\mu\text{m/s}$. Coincident with this decrease, enrichment of BODIPY²⁻ commenced and i_{BPE} increased from 55 to 190 nA. The underlying reason for this increase is the main point of this study and will be discussed in the next subsection.

Further changes to the PDF rate, initiated with additional increments of solution to the cathodic reservoir, result in progressive changes in i_{BPE} and movement of the enriched band away from the BPE. Specifically, 2.0 μL aliquots of solution were added to the cathodic reservoir every 60 s starting at $t = 220$ s and continuing until 460 s. Each aliquot corresponds to a decrease in the PDF rate of ~ 21 $\mu\text{m/s}$ and results in the enriched band moving ~ 200 μm closer to the anodic reservoir. A corresponding series of stepwise decreases in i_{BPE} are observed (Figure 1b). Note, however, that the precise change in the total flow rate and movement of the enriched band varies slightly with each addition of buffer due to imperfectly shaped reservoirs and changes in electroosmotic flow rate induced by the PDF. This is a minor point, but nevertheless a complete discussion is provided in the Supporting Information (Figure S1).

To demonstrate that changes in the position of the enriched band and i_{BPE} are reversible, the foregoing experiment was reversed by adding 2.0 μL aliquots of solution to the anodic reservoir every 60 s starting at $t = 460$ s. This results in the enriched band moving ~ 200 μm closer to the BPE for each 2.0 μL addition and stepwise increases in i_{BPE} (Figure 1b). The key trends illustrated in Figure 1b are that the formation of the enriched band results in a sharp increase in i_{BPE} , and that i_{BPE} decreases and increases as the enriched band moves away from and toward the BPE, respectively. One final point: the BODIPY²⁻ tracer is itself not electroactive over the range of potentials relevant to this study, and therefore it does not contribute directly to i_{BPE} .

Figure 1c shows the relationship between the position of the enriched BODIPY²⁻ band and i_{BPE} , measured over the course of eight experiments and using different microfluidic devices. Here, the horizontal axis represents the distance between the cathodic edge of the BPE and the edge of the enriched band closest to the BPE. These data demonstrate the consistent increase in i_{BPE} recorded as the enriched BODIPY²⁻ band moves closer to the BPE. Accordingly, i_{BPE} can be used to estimate the longitudinal position of the enriched band. As discussed in the Supporting Information, however, there is no relationship between the magnitude of i_{BPE} and the concentration of the enriched band (Supporting Information Figure S2).

Elucidation of the Source of BPE Current Changes. Previously we reported that water reduction at the cathodic pole of the BPE results in neutralization of TrisH⁺ buffer cations according to eqs 4 and 5.³⁻⁵



The resulting formation of a region of lower conductivity (depletion region) is critical to the formation of a steep electric field gradient and the subsequent enrichment process (Scheme 1). We have previously shown that the potential difference between pairs of microbands situated in the vicinity of the BPE (Figure 1a) can be used to construct a map of this gradient.³ The dashed line in Figure 2a shows that when the total flow rate is too fast for enrichment to commence there is

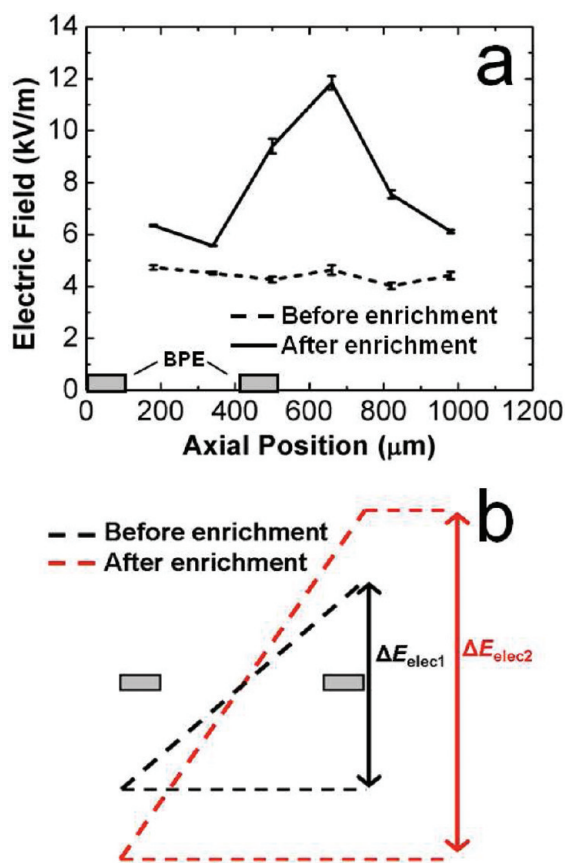


Figure 2. (a) Measured electric field profiles in the microchannel in the region near the BPE upon enrichment of BODIPY²⁻ by application of $E_{\text{tot}} = 25.0$ V. Profiles were measured before (dashed line) and after (solid line) enrichment by modulating the flow rate. Error bars indicate the standard deviation from the mean for three replicate measurements. (b) Representation of the change in ΔE_{elec} upon initiation of enrichment. Depletion of TrisH⁺ in the vicinity of the BPE results in a higher solution resistance and hence an increase in ΔE_{elec} . The initial concentrations in the microchannel were 5.0 mM Tris-HCl (pH 8.1) and 1.0 μM BODIPY²⁻. The BPE had a length of 500 μm .

essentially no field gradient. However, when the flow rate is reduced (by decreasing the PDF rate), thereby initiating enrichment, a gradient develops (solid line in Figure 2a). Significantly, part of the elevated electric field is directly above the BPE (0–500 μm in Figure 2a). This means that ΔE_{elec} is higher after enrichment is observed, and therefore a greater driving force for the oxidation and reduction of water exists at the poles of the BPE (Figure 2b). This observation explains the sharp increase in i_{BPE} upon the initiation of enrichment (Figure 1b).

Numerical simulations were used to confirm the locations of TrisH⁺ depletion and the elevated electric field. Specifically, Figure 3a shows the simulated TrisH⁺ concentration profile in the microchannel. During enrichment, the depletion region is located over the BPE and just to its right. The elevated TrisH⁺ concentration over the anodic pole of the BPE arises from protonation of Tris due to oxidation of water (proton formation). Figure 3a also shows that the location of TrisH⁺ depletion is a function of the total flow rate (i.e., PDF + EOF). Therefore, when the depletion region moves, the location of the field gradient (Figure 3b), and hence the location of enrichment, also moves. Additionally, Figure 3b shows that when the enriched

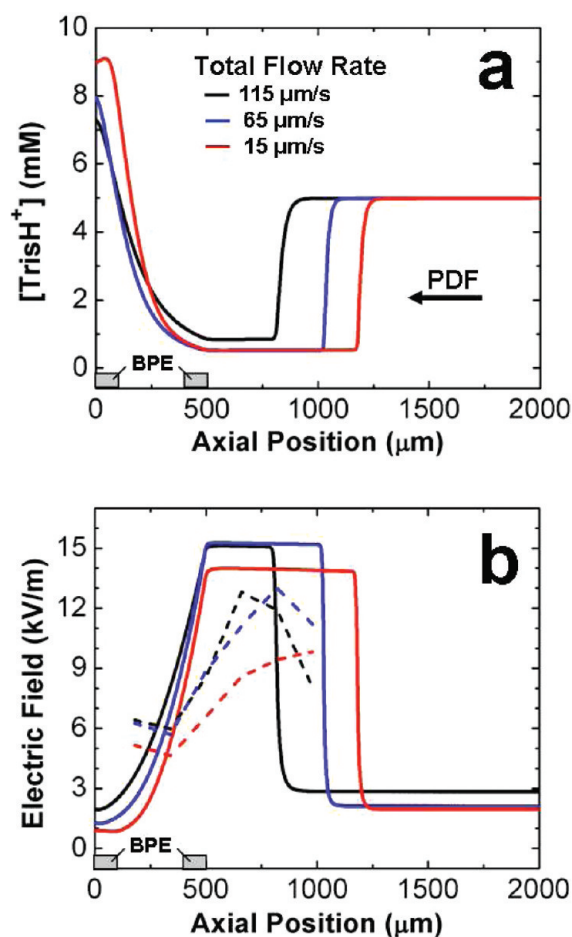


Figure 3. (a) Simulated TrisH⁺ concentration profiles. (b) Simulated (solid line) and measured (dashed line) electric field profiles during a BODIPY²⁻ enrichment experiment. The BPE spans the range from 0 to 500 μm . The initial concentrations in the microchannel were 5.0 mM Tris-HCl (pH 8.1) and 1.0 μM BODIPY²⁻. $E_{\text{tot}} = 25.0$ V.

band moves away from the BPE, the total electric field strength over the BPE decreases (lower ΔE_{elec}), which explains the decrease in i_{BPE} recorded upon moving the enriched band away from the BPE (Figure 1b). The simulated electric field profiles (Figure 3b, solid lines) are qualitatively similar to those determined experimentally (Figure 3b, dashed lines) for a given total flow rate. Quantitative differences are the result of necessary approximations used for the simulations, and these are discussed in detail in the Supporting Information.

Further evidence for the formation and movement of the depletion region can be obtained by examining the total current flowing through the microchannel (i_{tot}). Figure 4 shows i_{tot} measured as a function of time during an enrichment experiment. At $t = 0$ s, $E_{\text{tot}} = 25.0$ V was applied resulting in $i_{\text{tot}} = 380$ nA. At this time, the total flow rate toward the cathodic reservoir was too fast for enrichment to occur (similar to the initial conditions used in Figure 1b), so i_{BPE} is quite low (~ 20 nA). Next, at $t = 60$ s, enrichment was initiated by decreasing the PDF rate. This results in an increase in i_{BPE} , just as was noted in Figure 1b. Simultaneously, i_{tot} decreases due to the significant increase in solution resistance (R_{sol}) caused by the formation of the depletion region at the BPE. Next, between $t = 100$ and 175 s, the enriched band was moved toward the anodic reservoir by sequential additions of solution to

the cathodic reservoir. Each addition of solution results in a decrease in i_{BPE} . Simultaneously, i_{tot} decreases due to the expansion of the depletion region as the enriched band moves toward the anodic

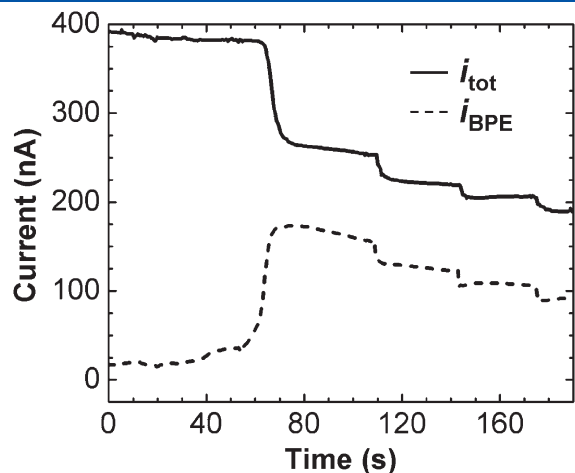


Figure 4. i_{tot} (solid line) and i_{BPE} (dashed line) as a function of time for an enriched BODIPY²⁻ band being formed and moved toward the anodic reservoir by modulation of the total flow rate. The initial concentrations in the microchannel were 5.0 mM Tris–HCl (pH 8.1) and 1.0 μM BODIPY²⁻. The BPE had a length of 500 μm . $E_{\text{tot}} = 25.0$ V.

reservoir (Figure 3a). The temporal relationship of the changes in i_{BPE} and i_{tot} in Figure 4 provide evidence of the responsiveness of i_{BPE} to the formation and movement of an enriched band.

Effect of Enriched Band Position on a Secondary BPE. To further illustrate the ability of the depletion region to modulate i_{BPE} , its influence on the current passing through a secondary BPE was monitored. For these experiments, the secondary BPE was placed between the enrichment BPE and the anodic reservoir by connecting a second pair of microbands (Figure 5a). Figure 5b shows i_{BPE} for the secondary BPE when an enriched band (formed at the enrichment BPE) is moved over the secondary BPE and to the right of it by changing the PDF rate. Faradaic reactions were induced in the secondary BPE when the enriched band was above or to the right of the secondary BPE ($t = 50$ s), and they were switched off again when the enriched band was pushed back to the left of the secondary BPE ($t = 175$ s).

When the enriched band was located between the enrichment BPE and the secondary BPE (Figure 5d, solid line), the electric field to the right of the enriched band (including the secondary BPE region) was relatively low in magnitude. The secondary BPE experienced an electric field strength of ~ 4.0 kV/m corresponding to a ΔE_{elec} of ~ 1.44 V for the secondary BPE (360 μm in length). This is insufficient to induce faradaic reactions at the secondary BPE (see the Supporting Information). However, as the position of the enriched band is pushed further to the right such that the enriched band is located over the secondary BPE

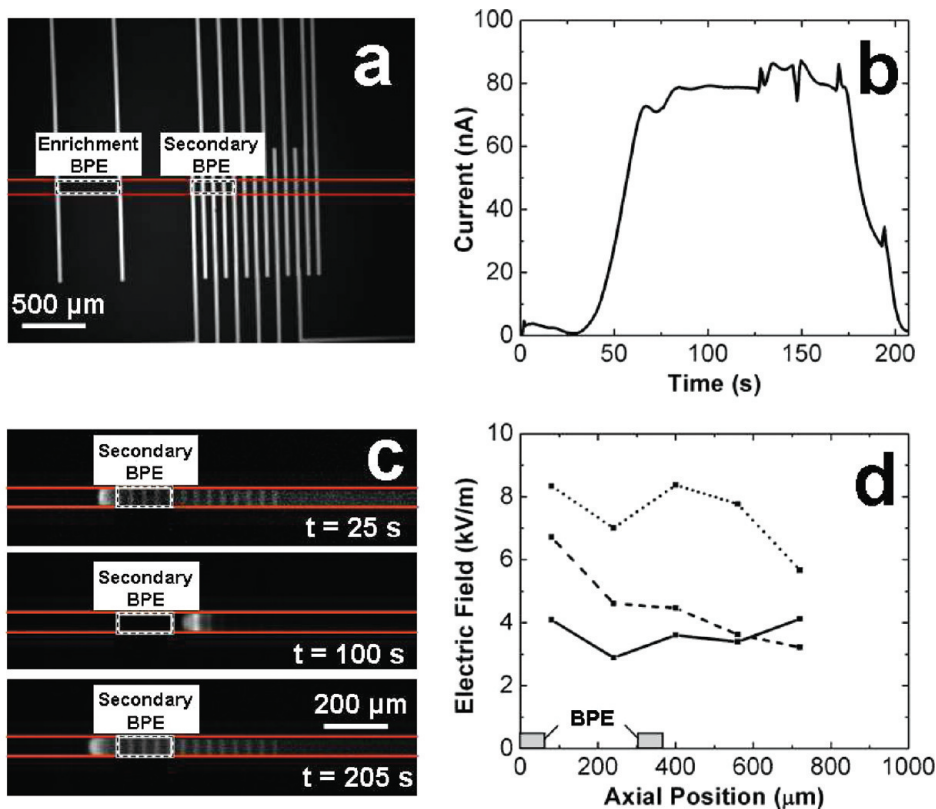


Figure 5. (a) Optical micrograph showing a device containing an enrichment BPE and a secondary detection BPE. (b) i_{BPE} as a function of time showing the increase in current through the secondary BPE as an enriched BODIPY²⁻ band is moved to the left, to the right, and back to the left of the BPE by changing the total flow rate. (c) Fluorescence micrographs showing the position of the enriched band after 25, 100, and 205 s for the experiment in panel b. (d) Measured electric field profiles in the vicinity of the secondary BPE during the experiment in panel b. The secondary BPE spans the region from 0 to 360 μm . The profiles were recorded when the enriched band resided to the left of the secondary BPE (solid line), above the secondary BPE (dashed line), and to the right of the secondary BPE (dotted line). The initial concentrations in the microchannel were 5.0 mM Tris–HCl (pH 8.1) and 1.0 μM BODIPY²⁻. The enrichment and secondary BPEs had lengths of 500 and 360 μm , respectively. $E_{\text{tot}} = 25.0$ V.

(Figure Sd, dashed line) and to the right of the secondary BPE (Figure Sd, dotted line), the electric field strength over the BPE increases significantly. This increase corresponds to the movement of the depletion region over the secondary BPE such that a greater potential drop occurs in this region. An electric field strength of 8.0 kV/m corresponds to a ΔE_{elec} of ~ 2.9 V at the secondary BPE, which is sufficient to induce faradaic reactions at the secondary BPE. This result demonstrates that the depletion region can exert control over the faradaic reactions at a secondary BPE. Important information about the location of the enriched band can be determined from such measurements.

SUMMARY AND CONCLUSIONS

We have described a method for monitoring the formation and position of an enriched anionic tracer band in a microchannel. Specifically, formation of an enriched band is coincident with a sharp increase in i_{BPE} , and the position of the enriched band correlates to the magnitude of i_{BPE} . We used both experiments and simulations to explain the underlying mechanism for this observation.

Looking to the future, the findings reported here represent an important step toward our ultimate goal of developing a lab-on-a-chip device capable of simultaneously enriching, separating,⁴ and quantifying analytes on the microliter scale and without the need for labels. Having easy access to the location of enriched bands also provides a simple means for integrating more quantitative detection methods, for example mass spectrometry, to this type of microdevice. Results relating to such studies will be reported in due course.

ASSOCIATED CONTENT

S Supporting Information. Discussion of the faradaic reactions occurring at the BPE, description of the employed numerical approach for simulation of buffer and faradaic reactions, a note on the influence of total flow rate on the formation of a depletion region, a note on the variability of influence of PDF rate on enriched band position, a control experiment demonstrating the relationship between enriched band concentration and i_{BPE} , and a note on the influence of BPE length on initiation of faradaic reactions. This material is available free of charge via the Internet at <http://pubs.acs.org>.

AUTHOR INFORMATION

Corresponding Author

*E-mail: crooks@cm.utexas.edu (R.M.C.); tallarek@staff.uni-marburg.de (U.T.).

Present Address

[†]Department of Chemistry, University of Washington, Box 351700, Seattle, Washington 98195-1700, United States.

ACKNOWLEDGMENT

We gratefully acknowledge support from the Chemical Sciences, Geosciences, and Biosciences Division, Office of Basic Energy Sciences, Office of Science, U.S. Department of Energy (contract no. DE-FG02-06ER15758). We also thank the Robert A. Welch Foundation (Grant F-0032) for sustained support. Simulations were run at the "Leibniz-Rechenzentrum der Bayerischen Akademie der Wissenschaften" (Garching, Germany), supported by project HLRB pr26wo.

MAJOR SYMBOLS

E_{onset}	onset potential, V
ΔE_{elec}	potential difference between two ends of the bipolar electrode, V
E_{tot}	applied voltage between the driving electrodes, V
i_{BPE}	current through the BPE, A
i_{tot}	total current through the microchannel, A
l_{channel}	total microchannel length, m
l_{elec}	total BPE length, m
R_{sol}	total solution resistance in the microchannel, Ω
μ_{EOF}	electroosmotic mobility, $\text{m}^2/(\text{V s})$
v_{EOF}	electroosmotic velocity, $\mu\text{m/s}$

REFERENCES

- Anand, R. K.; Sheridan, E.; Hlushkou, D.; Tallarek, U.; Crooks, R. M. *Lab Chip* **2011**, *11*, 518–527.
- Anand, R. K.; Sheridan, E.; Knust, K. N.; Crooks, R. M. *Anal. Chem.* **2011**, *83*, 2351–2358.
- Perdue, R. K.; Laws, D. R.; Hlushkou, D.; Tallarek, U.; Crooks, R. M. *Anal. Chem.* **2009**, *81*, 10149–10155.
- Laws, D. R.; Hlushkou, D.; Perdue, R. K.; Tallarek, U.; Crooks, R. M. *Anal. Chem.* **2009**, *81*, 8923–8929.
- Hlushkou, D.; Perdue, R. K.; Dhopeswarkar, R.; Crooks, R. M.; Tallarek, U. *Lab Chip* **2009**, *9*, 1903–1913.
- Dhopeswarkar, R.; Hlushkou, D.; Nguyen, M.; Tallarek, U.; Crooks, R. M. *J. Am. Chem. Soc.* **2008**, *130*, 10480–10481.
- Ko, S. H.; Kim, S. J.; Cheow, L. F.; Li, L. D.; Kang, K. H.; Han, J. *Lab Chip* **2011**, *11*, 1351–1358.
- Mir, M.; Homs, A.; Samitier, J. *Electrophoresis* **2009**, *30*, 3386–3397.
- Salehi-Reyhani, A.; Kaplinsky, J.; Burgin, E.; Novakova, M.; Demello, A. J.; Templer, R. H.; Parker, P.; Neil, M. A. A.; Ces, O.; French, P.; Willison, K. R.; Klug, D. *Lab Chip* **2011**, *11*, 1256–1261.
- Du, Y.; Chen, C. G.; Zhou, M.; Dong, S. J.; Wang, E. K. *Anal. Chem.* **2011**, *83*, 1523–1529.
- Foote, R. S.; Khandurina, J.; Jacobson, S. C.; Ramsey, J. M. *Anal. Chem.* **2005**, *77*, 57–63.
- Khandurina, J.; Jacobson, S. C.; Waters, L. C.; Foote, R. S.; Ramsey, J. M. *Anal. Chem.* **1999**, *71*, 1815–1819.
- Ramsey, J. D.; Collins, G. E. *Anal. Chem.* **2005**, *77*, 6664–6670.
- Chang, W.; Komazu, T.; Korenaga, T. *Anal. Lett.* **2008**, *41*, 1468–1476.
- Wen, J.; Wilker, E. W.; Yaffe, M. B.; Jensen, K. F. *Anal. Chem.* **2010**, *82*, 1253–1260.
- Macounova, K.; Cabrera, C. R.; Holl, M. R.; Yager, P. *Anal. Chem.* **2000**, *72*, 3745–3751.
- Hofmann, O.; Che, D. P.; Cruickshank, K. A.; Muller, U. R. *Anal. Chem.* **1999**, *71*, 678–686.
- Tang, G. Y.; Yang, C. *Electrophoresis* **2008**, *29*, 1006–1012.
- Ge, Z. W.; Wang, W.; Yang, C. *Lab Chip* **2011**, *11*, 1396–1402.
- Kelly, R. T.; Woolley, A. T. *J. Sep. Sci.* **2005**, *28*, 1985–1993.
- Burke, J. M.; Ivory, C. F. *Electrophoresis* **2010**, *31*, 893–901.
- Koegler, W. S.; Ivory, C. F. *J. Chromatogr., A* **1996**, *726*, 229–236.
- Petsev, D. N.; Lopez, G. P.; Ivory, C. F.; Sibbett, S. S. *Lab Chip* **2005**, *5*, 587–597.
- Humble, P. H.; Kelly, R. T.; Woolley, A. T.; Tolley, H. D.; Lee, M. L. *Anal. Chem.* **2004**, *76*, 5641–5648.
- Shen, M.; Yang, H.; Sivagnanam, V.; Gijs, M. A. M. *Anal. Chem.* **2010**, *82*, 9989–9997.
- Chun, H. G.; Chung, T. D.; Ramsey, J. M. *Anal. Chem.* **2010**, *82*, 6287–6292.
- Wang, Y. C.; Stevens, A. L.; Han, J. Y. *Anal. Chem.* **2005**, *77*, 4293–4299.

- (28) McDonald, J. C.; Duffy, D. C.; Anderson, J. R.; Chiu, D. T.; Wu, H. K.; Schueller, O. J. A.; Whitesides, G. M. *Electrophoresis* **2000**, *21*, 27–40.
- (29) Hellmich, W.; Regtmeier, J.; Duong, T. T.; Ros, R.; Anselmetti, D.; Ros, A. *Langmuir* **2005**, *21*, 7551–7557.
- (30) Higuera, F. J.; Succi, S.; Benzi, R. *Europhys. Lett.* **1989**, *9*, 345–349.
- (31) Warren, P. B. *Int. J. Mod. Phys. C* **1997**, *8*, 889–898.
- (32) Capuani, F.; Pagonabarraga, I.; Frenkel, D. *J. Chem. Phys.* **2004**, *121*, 973–986.